Influence of a macroporous β-TCP structure on human mesenchymal stem cell proliferation and differentiation in vitro

Shaan Chamary, Liliana Grenho, Maria Helena Fernandes, Franck Bouchart, Fernando Jorge Monteiro, Jean-Christophe Hornez

Open Ceramics 7 (2021) 100141

Contents lists available at ScienceDirect

Open Ceramics

journal homepage: www.editorialmanager.com/oceram

Influence of a macroporous β-TCP structure on human mesenchymal stem cell proliferation and differentiation *in vitro*

Shaan Chamary [a,*], Liliana Grenho [b], Maria Helena Fernandes [b], Franck Bouchart [a], Fernando Jorge Monteiro [c,d,e], Jean Christophe Hornez [a]

[a] Université Polytechnique Hauts-de-France, EA 2443 - Laboratoire des Matériaux Céramiques et Procédés Associés, Boulevard Charles de Gaulle, 59600, Maubeuge, France
[b] Bone Lab, Faculty of Dental Medicine, U. Porto, Rua Dr. Manuel Pereira da Silva 4200-393, Porto, Portugal
[c] Instituto de Engenharia Biomédica, Rua Alfredo Allen, 208, 4200-135, Porto, Portugal
[d] Universidade Do Porto, Faculdade de Engenharia, Departamento de Engenharia Metalúrgica e de Materiais, Rua Dr.Roberto Frias S/n 4200-465, Porto, Portugal
[e] I3S- Instituto de Investigação e Inovação Em Saúde, Rua Alfredo Allen, 208, 4200-135, Porto, Portugal

ARTICLE INFO

Keywords:
β-tricalcium phosphate
Macroporous scaffolds
Human mesenchymal stem cells
Proliferation
Differentiation
In vitro

ABSTRACT

This work aims at studying the links between a porous scaffold in β-TCP and its impact on cell differentiation and proliferation *in vitro*. β-TCP was synthesized by aqueous precipitation. The shaping methods were chosen for their ability to generate original structures with the potential to positively influence cell behaviour. The impregnation of polymeric structure (PS) yielded an interconnected network of spherical pores, stereolithography (3D) yielded a network of interconnected diamond shaped pores and freeze casting (FC) yielded a network of parallel ellipsoidal channel-like pores. Two different trends emerged from the human mesenchymal stem cell culture: 3D and PS seems to promote surface proliferation whereas the freeze casted samples promoted cell penetration, bulk colonization, expression of key osteoblastic genes (RunX-2, ALP, BMP-2, BGLAP and Collagen) and alkaline phosphatase activity. The architectural features created by freeze casting positively influenced human mesenchymal stem cells behaviour *in vitro*.

1. Introduction

Calcium phosphates have been successfully used as bone substitutes for decades mostly because their chemical composition is very close to that of the mineral phase of bone tissues. Furthermore, these biocompatible compounds induce the same biological responses as bone [1,2] such as osteoconduction and even osteoinduction in some cases [3,4].

It is today widely accepted that structural features, such as porosity, pore shape, interconnectivity and topography, impact cell behaviour *in vivo* and *in vitro* [5]. They can be designed and tailored to elicit a controlled and guided healing process. Cells are sensitive to their chemical and physical environment. For instance, two dimensional cell culture systems will not yield the same cellular genetic signature as its three dimensional counterpart [6,7]. Through a phenomenon known as mechanotransduction, cells will translate mechanical or topographical stimuli into biological events such as increased proliferation or differentiation. This property can be used concomitantly with or as an alternative to biochemical stimulation. Therefore, optimizing an implant design will improve bone reconstruction and healing. Architectural features are more stable *in vivo* than chemical modifications or functionalization and will impact cell behaviour in very localized areas [8]. Moreover, the high dosages needed for certain chemicals to be efficient can induce problems such as tumorigenicity [9,10].

Porosity will affect an implant's bioactivity and mechanical properties [11]. An open interconnected porous network will allow cells and body fluids to move freely inside the implant, hence facilitating interactions with the material. It has been shown, *in vivo* and *in vitro*, that high porosity volumes tend to yield better results than lower ones [12–14]. The array of porous volume tested that yielded positive results ranges from 40% to 70%. However, in order to preserve mechanical strength, low porosity volume and homogeneous spatial pore distribution should be favoured [15]. Porosity will also impact specific surface area. During the first 48 h, cells are receptive to high specific surfaces which allowed early adhesion compared to samples with low specific surface area. However, this effect is quickly replaced (over 48 h) by cell migration [16].

Pore diameter is another key parameter. In some cases, it has even been shown that pore size has a larger impact over new bone synthesis

* Corresponding author.

https://doi.org/10.1016/j.oceram.2021.100141
Received 15 March 2021; Received in revised form 11 May 2021; Accepted 10 June 2021
Available online 17 June 2021

than pore volume [12]. Pore size and interconnection diameter are often chosen according to the largest circulating elements. Their diameter should at least be around a hundred microns [17–19]. Once again the range of pore size yielding positive results is broad. Active osteoconduction took place in pores ranging from 50 μm up to 400 μm. As pore size increases, osteoconduction seems to be more and more efficient [20,21]. Even when porous calcium phosphate is coupled with BMPs (Bone Morphogenetic Proteins), the optimal pore size seems to be over 300 μm as only unmineralized tissue can be found in lower diameter pores [22,23]. These previous results seem to stem from the fact that ossification mechanisms vary according to vascularization efficiency which is itself dependent on pore size [24]. Adequate blood irrigation is compulsory for a positive outcome as it will supply cells with oxygen, nutrients and regulatory molecules while evacuating waste products [25]. Pore sizes inferior to 300 μm do not favour vascularization hence the osteochondral ossification. Over 300 μm, bone formation is efficient and it seems that over this value, size has very little impact over cell behaviour [26].

Microporosity has an early impact over cell adhesion and even seems to be a requirement for new bone formation [27,28]. However, these results have been challenged by a number of publications. Microporosity can cause the specific surface area to raise thus increasing interactions between the material and its environment. In some cases, it contributed to a harsh ionic environment and to deleterious growth conditions [29–31]. Other studies questioned the necessity of microporosity, as over long periods of time (28 days), cell adhesion and proliferation are the same on microporous and non-microporous samples [32]. Alongside microporosity, micrometric and nanometric structures can be potent topographic stimuli for proliferation and/or differentiation [8,33–37].

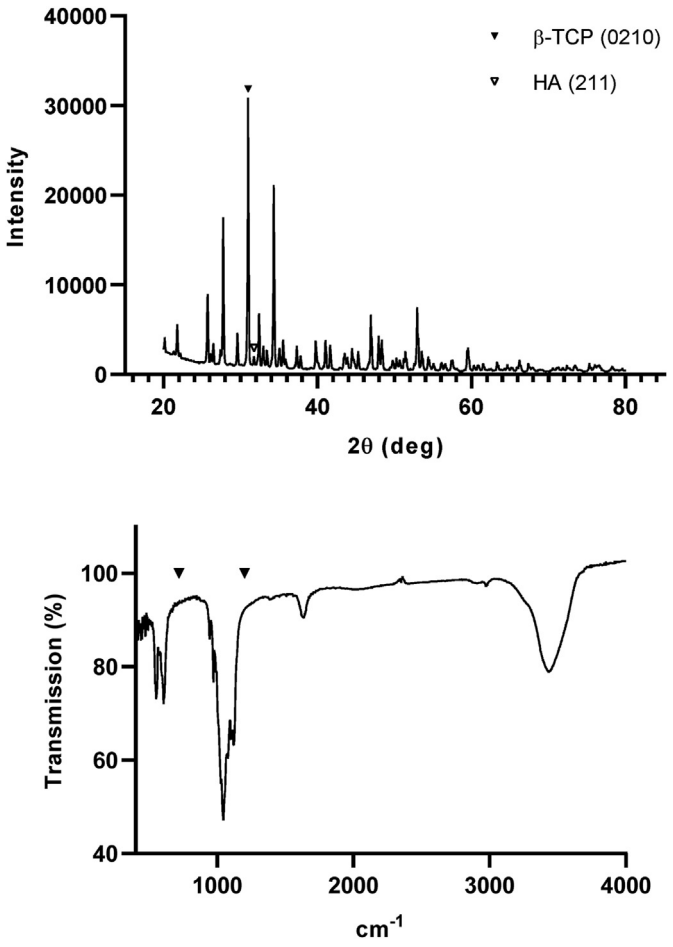

Fig. 1. XRD (CuKα) analysis used for phase quantification (top graph) & FT-IR spectra without calcium pyrophosphate bands at 720 cm^{-1} and 1200 cm^{-1} (bottom graph).

Literature shows that to improve an implant's efficiency, studies should focus on architectural cues such as pore topography and geometry. Depending on pore shape and size cells will adopt a specific behaviour. It has been shown that cell invasion and growth occurs faster in narrow pores thanks to curvature driven growth [38–40]. The narrower the pores are, the larger the amount of newly formed tissue is [41]. Furthermore, pore angle opening will also affect cell differentiation [42,43].

Literature concerning topographically and architecturally induced cell behaviour is abundant. However, no consensus has been met and only broad guidelines can be identified. In order to maximize the chances of positive cell stimulation, implants must feature a network of interconnected concave pores presenting acute angles and an adequate topography. Its porous volume should be kept to a minimum for mechanical reasons. In order to generate such structures, shaping methods should be carefully chosen and controlled. Many ceramic processing and shaping techniques have been developed for an increasing demand for porous material [44,45] And we believe that one or more is bound to yield architectural cues to positively influence both cell proliferation and differentiation.

This study focuses on the impact of macroporous β-TCP architectures on the behaviour of human mesenchymal stem cells at the osteoprogenitor stage *in vitro*. Three different shaping methods were chosen to manufacture macroporous structures, i.e. impregnation of a polymeric scaffold (PS) [46], stereolithography (3D) and freeze casting (FC) [47]. The different macroporous samples will serve as cell culture support and their effect on HMSC population will be analysed. SEM imaging, proliferation assay, enzymatic activity and osteoblastic gene expression analysis will enable us to identify links between architectural features and cell response. Furthermore, this study aims to show that the intrinsic structure generated by freeze casting might positively enhance osteoprogenitors differentiation and/or proliferation compared to classical structures.

2. Material and methods

2.1. β-TCP synthesis and shaping

β-TCP powder was synthesized through aqueous precipitation [46]. A diammonium phosphate solution $(NH_4)2HPO_4$ (Carlo Erba) is added in a controlled manner to a calcium nitrate solution $Ca(NO_3)_2$ (Brenntag), in a jacket reactor, under mechanical stirring. Thanks to a pH controller and a dosing pump (Blackstone BL7916, Hanna instruments), ammonia is injected into the mixture to maintain the slightly acidic (pH 6.3) condition needed. The reaction takes place at 30 °C over a period of 20 h. The suspension is then filtered and the solid matter is dried up at 90 °C for 48 h.

Purity was assessed through XRD and FT-IR according to the recommendations of the following ISO standards: ISO 13175–3 (2012) and ISO 13779–3 (2008).

Before shaping, the powder undergoes a thermal treatment at 850 °C for 3 h followed by a 3 h grinding process in order to break the agglomerates. These last steps will allow the transformation of the apatitic calcium phosphate into β-TCP and HA, the reduction of the powder's specific surface area and the elimination of residual ammonium nitrate, NH_4NO_3.

Three shaping methods were chosen for the manufacturing of discs (11 mm in diameter and 3 mm in height).

Impregnation of a polymeric scaffold (PS): the manufacturing of these samples relied on the work of Descamps et al. (DES08). The polymeric scaffolds are made out of partially fused polymethylmetacrylate beads (PMMA, Diakon TM Ineos Acrylics). In our case the size range chosen was between 500 and 600 μm with interconnections of 150 μm before sintering. Through SEM imaging, interconnection diameter was observed and verified.

The scaffold was impregnated in a plaster mould by an aqueous slurry composed of 65 % wt. of dry matter. Before sintering, the porogen was cleanly eliminated via a slow thermal treatment: 220 °C for 20 h followed by 250 °C for 4 h. Sintering took place at 1100 °C for 3 h, the heating and cooling rate being 5 °C/min.

Stereolithography (3D): this method relies on the photosensitive properties of a slurry composed of 65 % wt. of dry matter and 35 % wt. of acrylic resin (Cryoberyl Software). The latter is a cocktail of photo-initiators, stabilizing and dispersing agents. Mixing took place in a planetary ball mill (Retsch) for 30 min at a 100 RPM.

The digital version of the sample was designed thanks to the software Catia (Dassault Systèmes). Slicing and placement of the support structures were done through Workshop (Datatree3D). The data was then transferred to the printing software (Cryoceram, Cryoberyl Software) and apparatus (CryoCeram printer, Cryoberyl Software). A dynamic mask projection allowed localized polymerization and sample printing from bottom to top. Curing energy was set to 5 mW/cm^2 and slice thickness to 50 μm.

Printing is followed by washing steps in order to remove unpolymerized matter. The samples are then debounded and sintered at 1100 °C for 3 h, the heating and cooling rate being 5 °C/min.

Freeze casting (FC): slurries were prepared by mixing in a Turbula® mixer for 30 min, distilled water, 57 % wt. of powder and 2.25 % wt. of dispersant (Dolapix CE64, Zschimmer & Schwarz) for 24 h with milling balls. The suspension was then filtered and transferred to another container where 1.5 % wt. of binding agent (Polyethylene glycol MW1000) was added.

The mould was made out of a brass frustoconical base and a Teflon® body glued together with low temperature resistant silicone glue. The mould was placed onto the freezing device (Air liquid, Freezal NH104003) and allowed to cool down to −20 °C at the rate of 1 °C/min. In order to maximize heat transfer between the device and the mould, thermal paste (Assman WSW component) was applied. When −20 °C was reached, 7 ml of suspension was poured into the mould. The temperature was dropped to −40 °C and maintained until complete suspension freezing. Water freezing takes place from bottom to top. After unmoulding, samples were freeze dried for 24 h (HETO CD8, Thermo Fisher Scientific), before being sintered at 1100 °C for 3 h, the heating and cooling rate being 5 °C/min.

2.2. Material characterization

Material composition was analysed through XRD (Panalytical DW/3040/60 - Copper tube) and FT-IR (Jasco, FT-IR 4600). HA weight percentage was calculated according to Equation (1) [48]. Prior to SEM imaging (FEI Quanta 400 FEG/ESEM), the macroporous structures were sputter coated with palladium/gold alloy. The average pore size and interconnections values were calculated over 200 manual measurements on SEM images (Image J). Porosity was calculated (Equation (2)) by hydrostatic weighing (RadWag AS220/X) in a standard device following the protocol described in ISO 623–2 - 1993. Surface areas were determined by a Brunauer-Emmet-Teller (BET) N_2 gas adsorption-desorption isotherms obtained on Micromeritics ASAP-2000 at 77 K. Samples were previously degassed at 400 °C under a dynamic vacuum of 13 mPa.

$$R_1 = \frac{I_{HA(211)}}{I_{TCP(0210)}} \% HA = \frac{R_1}{0,0111} \quad (1)$$

R1: intensity ratio
%HA: HA weight percentage of a biphasic powder (TCP/HA with TCP > 80% w/w)

$$\rho_{app} = \frac{M1}{M3 - M2} \times \rho L$$
$$\pi_a = \frac{M3 - M1}{M3 - M2} \times 100 \quad (2)$$

M1: mass of dry test piece
M2: apparent mass of the immersed test piece
M3: mass of the soaked test piece
ρapp: apparent density
πa: apparent porosity
ρL: water density

2.3. Biological characterization

Cell type: human mesenchymal stem cells (HMSC) were obtained from an orthopedic surgery procedure, after patient's informed consent. Bone marrow biopsy was broken down into small pieces so that it could be thoroughly washed with the following mixture: α-Minimum Essential Medium (α-MEM, Sigma) supplemented with antibiotics (Penicillin (10 units/ml) + Streptomycin (2.5 μg/ml), Sciencell), antifungal agents (Fungizone (2.5 μg/ml), Sigma) and 10% of foetal bovine serum (FBS, Gibco). The resulting cell suspension was cultured on a Petri dish over 10 days. Culture medium was renewed every 3 days. When 80% of confluence was reached, the cells were rinsed with PBS and enzymatically detached for further culture.

Flow cytometry analysis confirmed the presence of the following mesenchymal stem cells markers: CD90, CD105 and CD146 and the absence of CD45. Because of its pluripotency, the HMSC underwent histochemical staining: ALP stain for osteogenesis, oil red stain for adipogenesis and safranin O for chondrogenesis. The cells were positive for osteogenesis while being negative for adipogenesis and chondrogenesis. The HMSC population were identified as osteoprogenitors.

Cells were seeded onto sterile samples (Autoclave at 125 °C for 25 min in humid conditions at 1.5 atm relative pressure) into 24 well cell culture plates (2.10^4 cells/well) and incubated in a humidified atmosphere of 5% of CO_2 at 37 °C. In parallel, cells were cultured over the bare bottom surface of the well to serve as control. Culture medium was renewed every 3 days.

Evaluation techniques: cell metabolic activity was evaluated through

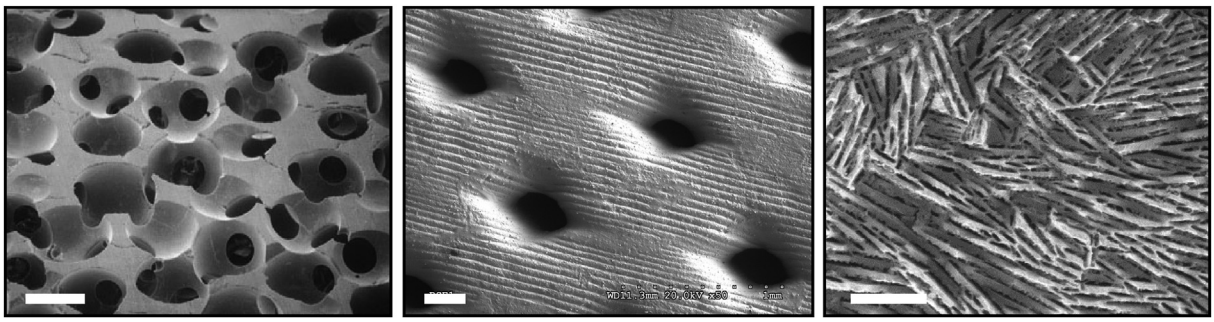

Fig. 2. SEM image of (from left to right) PS, 3D and FC. **Scale bars: 0.5 mm**.

a resazurin assay over a period of 35 days. Fresh medium with 10% of resazurin was added to the cells and incubated over 3 h. A 100 µl of medium was then transferred to a 96 well plate for fluorescence measurements (Synergy HT, Biotek). The excitation wavelength is 535 nm and the emission wavelength is 590 nm. The results are expressed in relative fluorescence unit (RFU).

For SEM pictures (FEI Quanta 400 FEG/ESEM), the cells were dehydrated in graded alcohol and hexamethysilazane (HDMS, Sigma) solution from 50 to 100%. The samples were then sputter coated with a palladium/gold alloy prior to imaging.

Alkaline phosphatase activity was measured through substrate hydrolysis in an alkaline environment (pH 10.5). *P*-nitrophenyl phosphate (Sigma) undergoes dephosphorilation thanks to alkaline phosphatase and is transformed into *P*-nitrophenol. Its concentration is measured in a plate reader at an absorbance of 405 nm. The results are normalized to total protein content and are expressed in nanomole of *P*-nitrophenol produced per microgram of protein.

Quantitative RT-PCR was performed to evaluate the osteoblastic differentiation of the HMSC cultured on the biomaterial. Cells cultured on tissue culture plate were set as the control group. At day 14 of culture, total RNA was extracted using TRIZOL® reagent (Invitrogen) and reverse transcribed into complementary DNA (cDNA) using iScript™ Adv cDNA Kit (BioRad). To analyse the expression of specific genes for osteoblastic differentiation, the expression of Runt-related transcription factor 2 (Runx-2), Alkaline Phosphatase (ALP), Collagen, type I (COL1A1), Bone morphogenetic protein 2 (BMP-2), Osteocalcin (BGLAP) was determined quantitatively in a PrimePCR™ custom plate, on a RT-PCR equipment (CFX96, BioRad) using iQTM SYBR® Green Supermix (BioRad). Glyceraldehyde-3-phosphate dehydrogenase (GAPDH) was used as the reference gene for normalization.

Statistical analysis: Triplicate analyses were performed for all experiments and the results are expressed as the arithmetic means ± standard deviation. The statistical analysis was conducted using one way analysis of variance. Levels of $p \leq 0.05$ were considered to be statistically significant. The software used was GraphPad Prism 8.0.1.

Table 1
Pore and interconnection sizes, porosity and surface area of the following samples: PS, 3D and FC.

Sample	Pore and interconnection size (µm)		Porosity (%)	Surface area (m^2/g)
PS	435 ± 58 (Pore) – 121 ± 22 (Interconnection)		65 ± 1	2.75
–	Small diameter	Long diameter	–	–
3D	202 ± 23	350 ± 23	50 ± 1	1.53
FC	54 ± 16	366 ± 200	51 ± 1	3.77

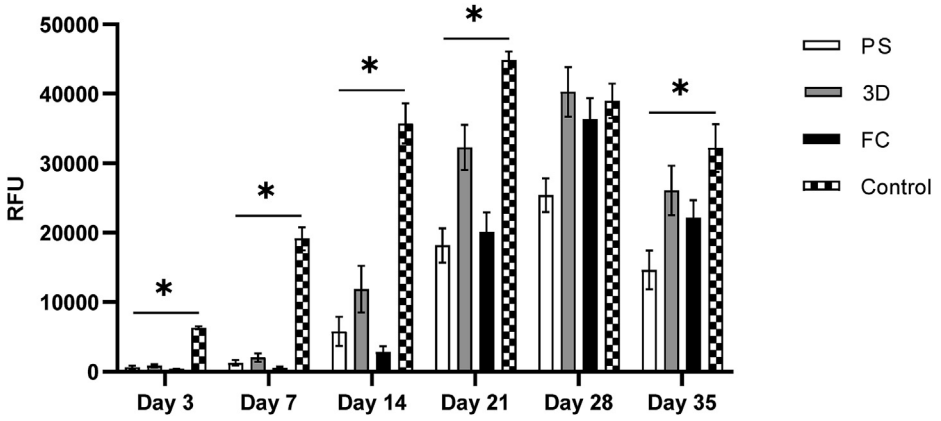

Fig. 3. Cell proliferation of HMSC cultured over PS, 3D and FC samples for 35 days, assessed by the Resazurin assay. An empty polystyrene well served as control and results are expressed in Relative Fluorescence Unit (RFU). *significantly different ($p \leq 0,05$).

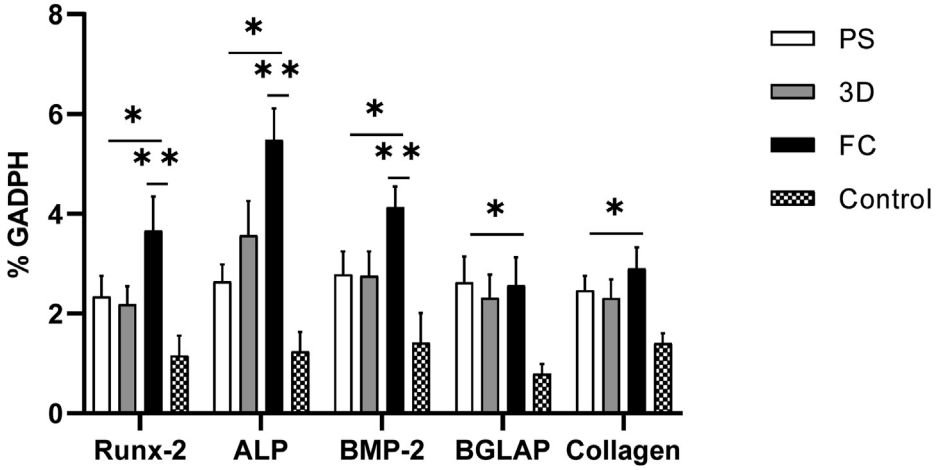

Fig. 4. RT-PCR analysis on HMSC cultured over PS, 3D and FC samples, at day 14. *Significantly different from control ($p \leq 0,05$); **significantly different from PS and 3D ($p \leq 0,05$).

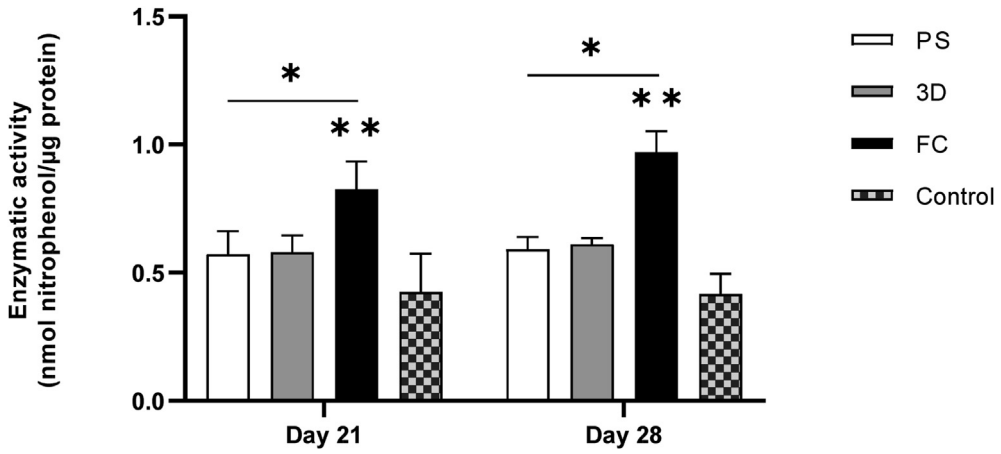

Fig. 5. Alkaline phosphatase activity of HMSC cultured over PS, 3D and FC samples measured over 14 days. Results are expressed in nanomole of nitrophenol per µg of protein. *Significantly different from control ($p \leq 0,05$); **significantly different from PS and 3D ($p \leq 0,05$).

3. Results

3.1. Material characterization

XRD (Fig. 1 top graph) confirms the presence of a few percent (2.7 ± 1%) of HA (peak (211) ($2\theta = 31,772°$) JCPDS 9–432) in β-TCP powder (peak (0210) ($2\theta = 31,027°$) JCPDS 09–0169). The absence of calcium pyrophosphate (bands at 720 cm^{-1} and 1200 cm^{-1}) was confirmed by FT-IR (Fig. 1 bottom graph).

SEM pictures (Fig. 2) show the architectural structure of the macroporous samples after shaping and sintering. PS exhibited an open network of interconnected spherical pores whereas 3D presented interconnected diamond shaped pores and the presence of parallel grooves on its surface. The frozen sample, FC exhibited a series of parallel tubular ellipsoidal pores perpendicular to the freezing direction.

The shaping parameters were chosen in order to yield samples with close properties (Table 1).

3.2. Biological characterization

3.2.1. Cell proliferation, gene expression, and ALP activity

Cell proliferation was assessed through resazurin assay, (Fig. 3). Cell growth occurred on every each sample. However, compared to the control, the samples exhibited a latency period up to 3–7 days. FC samples showed a longer latency phase between 7 and 14 days. Once latency phase over, exponential cell growth is visible from day 7 onwards on PS and 3D and a week later on FC. Cell confluence is reached 28 days later and on the 21st day for the control. Afterwards, cultures entered a senescence stage. 3D material hosted the largest HMSC population compared to PS and FC, with RFU values very close to those of the control on the 28th day. These results show that 3D material is more prone to cell proliferation by allowing faster growth and allowing cell confluence to be reached at its maximum compared to the control under the culture conditions tested.

Quantitative PCR analysis was performed on the 14th day of growth as it is the start of the exponential phase (Fig. 4). Five osteoblastic differentiation/maturation markers were chosen, RunX-2, ALP, COL-1A1 (collagen), BMP-2 and BGLAP. The results indicate that the control expresses an equivalent level of the 3 markers studied on the 14th day of growth. On the other hand, we observed RunX-2, ALP, BMP-2, COL-1A1 and BGLAP genes are expressed in a more important way compared to the control. In fact, an increase of 2 fold in the expression of the RunX gene in the presence of PS and 3D materials is observed, then by a factor 4 for the FC materials. The same is true for the expression of ALP and BMP2 genes. For the BGLAP and Col-1A1 genes, gene expression is twice as important for the three materials tested compared to the control. These results indicate that cell differentiation is more engaged on each sample than on the control. However, the FC samples allowed greater overexpression of the Runx, ALP and BMP2 genes. This indicates that the differentiation is more advanced on FC materials and seems to indicate a better mineralization in order to regenerate a new bone.

In order to confirm the increase in mineralization activities, we choose to assay the activity of alkaline phosphatase (Fig. 5). The results indicate more ALP activity for all samples compared to control. On PS and 3D samples, enzyme activity shows no variation over the testing period. The best ALP activities on FC samples were reached on the 21st an 28th day of culture and were significantly higher than those on PS and 3D samples. This result seems to confirm a mineralization more important (regeneration) on FC materials than on PS, 3D materials by osteoblast cells.

3.2.2. Cell migration through the porous structure

SEM pictures of the seeded materials were taken on the top (material surface) and within (cross-section) the samples, at days 21, 28 and 35.

PS samples showed a layer of cells and organic material that had grown over the surface and densified over time Fig. 6A, B, 21d; D, 28d). Well spread cells exhibiting cytoplasmic extensions and closely interacting with the rough surface topography were seen near and on the edge of the pores (Fig. 6C). Upon reaching the edge of the pores, cells continued to grow on the surface but did not migrate towards the pores (Fig. 6D, E, F). Instead, they exhibited a centripetal growth pattern with cell bridging between opposite sides of the pore in an attempt to cover the pores with a continuous cell layer (Fig. 6E and F). The appearance of the cell layer on Fig. 6F is suggestive of the formation of a well-organized cell layer with a mineralized matrix (white arrow). Cross-section pictures shows the circular-shaped interconnected pores and confirm that cells were not able to migrate into this structure (Fig. 6G, H, I). Only few isolated cells were visible inside the pores, probably those that adhered during the cell seeding (Fig. 6G and H). A high magnification image of the edge surface/pore (Fig. 6I) proves the difficulty of cell migration into the pores. An image of the unseeded sample (Fig. 6J) shows the smooth topography of the pores compared to the rough appearance of the surface (Fig. 6J, inset).

Samples 3D exhibited a dense cell layer that grew aligned to the parallel grooves on the surface (Fig. 7A, 21d; C, 28d). Over 21 days, the pores were almost completely covered with a cell layer (Fig. 7B and C). A high magnification image (Fig. 7D) shows an organized cell layer with a rich fibrillary matrix and suggests the presence of mineralized deposits (white arrow). Cross-section images indicated some cell penetration into the porous structure (Fig. 7E, F, H, I) that occurred preferentially at the corners of the pore (Fig. 7E, F, G). The significant difference between the dense cell surface layer and the poor cell migration is illustrated in

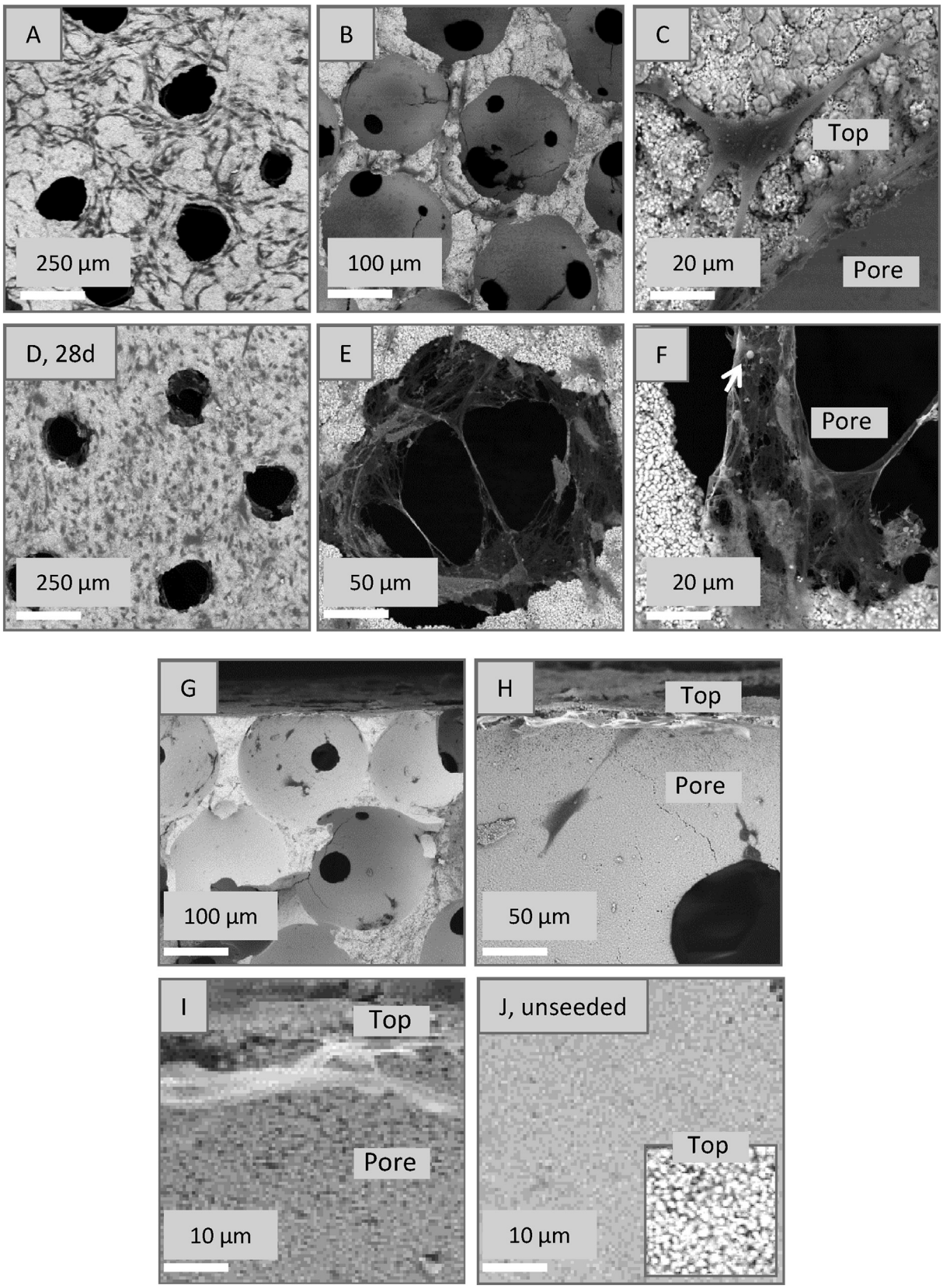

Fig. 6. SEM images of PS samples: surface (A–F) and cross section (G–J). Culture time: surface, 21 days (except image D: 28 days) and cross section, 28 days.

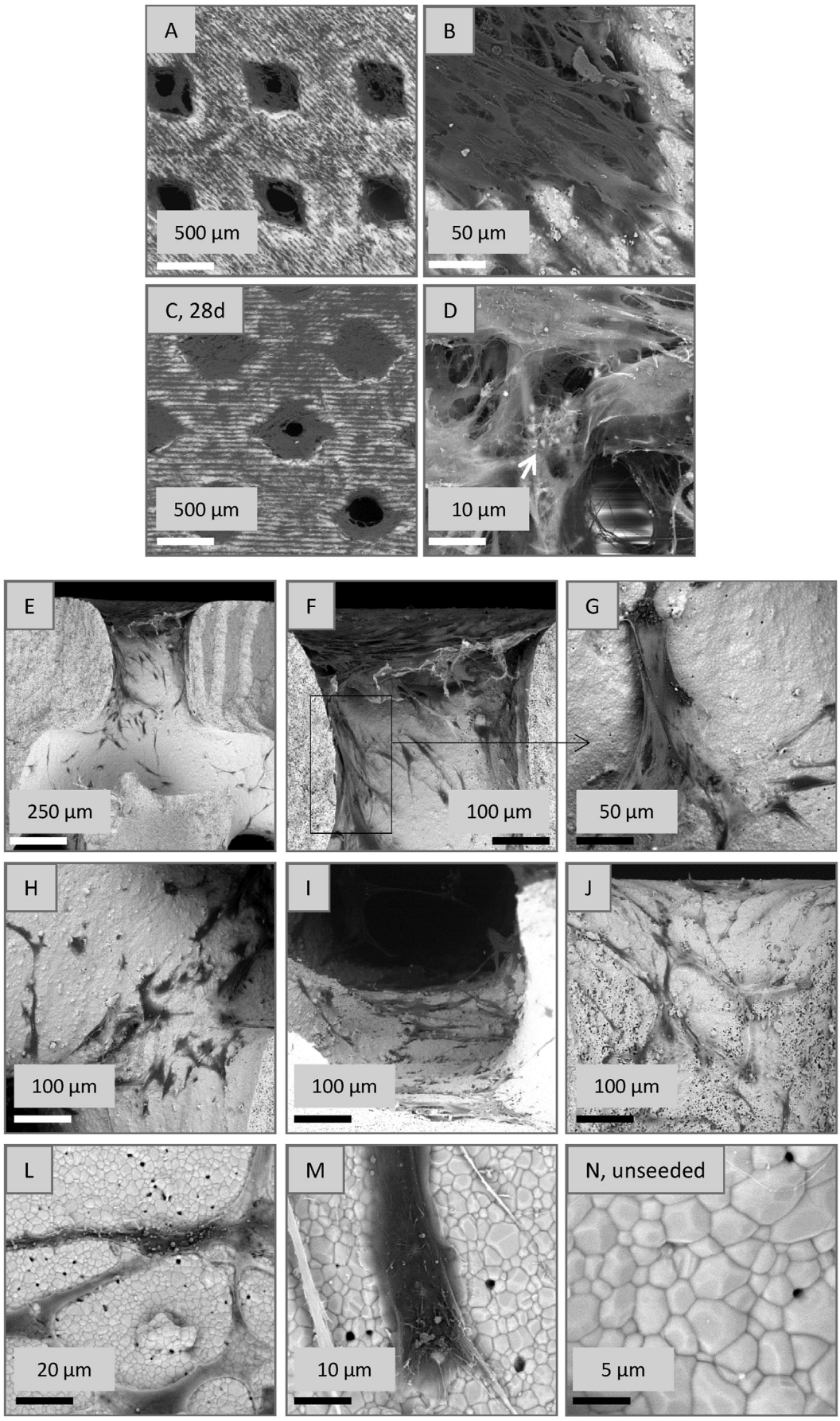

Fig. 7. SEM images of 3D samples: surface (A–D) and cross section (E–N). Culture time: surface, 21 days (except image C: 28 days) and cross section, 28 days.

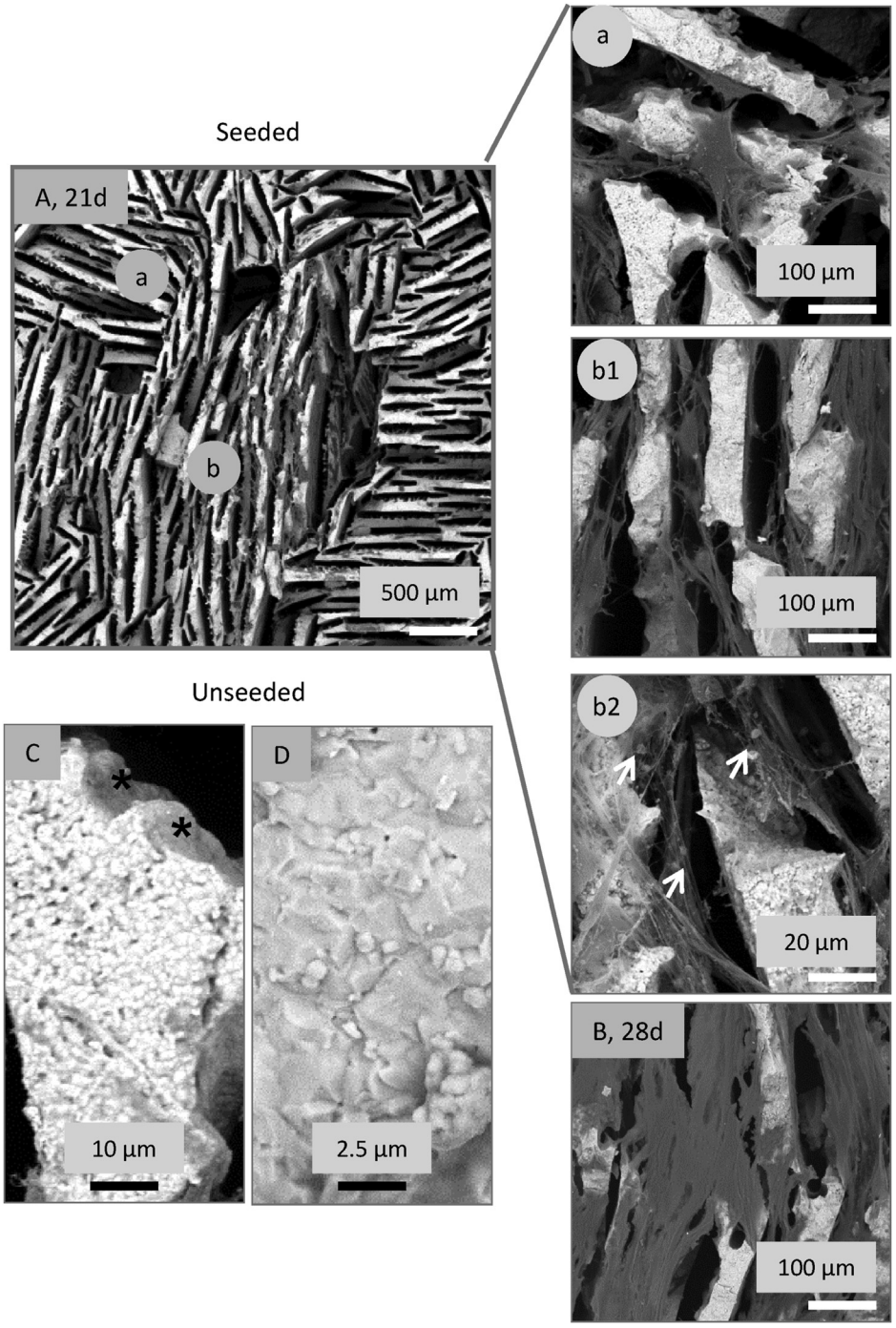

Fig. 8. SEM images of FC samples – Top.

Fig. 7F. Although some cell proliferation is observed inside the pores, cells presented an altered morphology, reflected by decreased spreading and, their inability to form a continuous sheet (Fig. 7H, I, J, L). A high magnification image (Fig 7M) depicts an elongated cell with limited spreading and only few filopodia. The unseeded sample shows a granular but smooth topography of the pore surface (Fig 7N).

The frozen samples yielded different results. FC also exhibits a surface cell layer (Fig. 8A, 21d; B, 28d). Higher magnification images show well-spread cells that closely adapted to the different orientations of the porous surface (Fig. 8A–a), with cytoplasmic extensions easily bridging pore walls (Fig. 8A–a, b1, b2) and covering the material surface and the pore space (Fig. 8A-b1, b2). These close interactions between the cells and the surface are specially evidenced on the higher magnification image (Fig. 8A-b2); this image shows a rich fibrilar cell layer and suggests the presence of a mineralized matrix. On the 28th day, the surface was almost completely covered by a cell layer (Fig. 8B).

The unseeded material shows a relatively homogeneous rough topography (Fig. 8C) that in high magnification exhibits irregular surface features that increased the surface area and favour the cell-material interactions (Fig. 8D). It is worth noting that the columnar-like material structures show regular protrusions (Fig. 8C, asterisks) that clearly function as anchoring points for the cells (Fig. 8A, b1, b2).

Regarding the cross-section, Fig. 9 depicts the cell penetration efficiency in the FC samples. Cell infiltration can be seen inside the porous network from the top to the bottom of the samples (Fig. 9A and B). High magnification images of Fig. 9B show the cell organization on the top

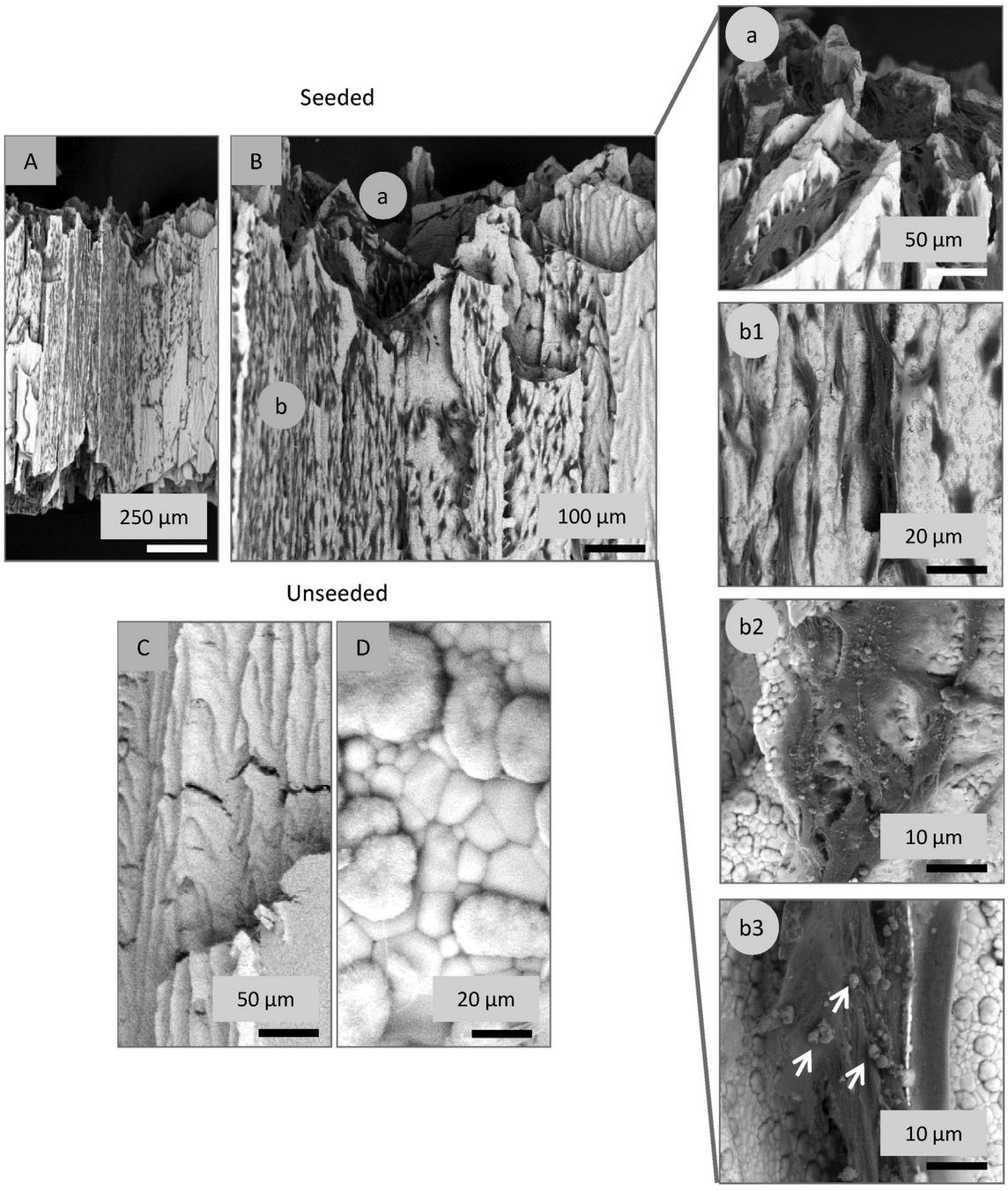

Fig. 9. SEM images of FC samples - Cross section.

(Fig. 9B–a) and within the tubular porous structure (Fig. 9B-b1, b2, b3). On the top of the material, cells almost covered the material at 21 days of culture and cells bridging the columnar structure are clearly visible (Fig. 9B–a). Within the scaffold, the ellipsoidal pore structure is completely filled with a continuous pore-driven cell layer (Fig. 9B-b1); higher magnification images show well-spread cells with cytoplasmic extensions, cell-to-cell communication on the material pore surface (Fig. 9B-b2) and an organized cell layer between two adjacent pore walls (Fig. 9-b3) with a strong suggestion of the presence of a mineralized matrix (Fig. 9-b3, white arrows).

Pore surface topography is shown in an unseeded sample; the pore wall depicts periodic protrusions along the pore length (Fig. 9C) and a higher amplification image (Fig. 9D) presents the irregular micrometric granular and rough topography of the pore surface.

4. Discussion

In this work, osteoprogenitors derived from HMSC were cultured under basal conditions on three different β-TCP porous samples *in vitro*. Cell proliferation and differentiation/maturation were assessed.

β-TCP was synthesized by aqueous precipitation (ISO 13779 and ISO 13175 compliance). The shaping methods were chosen for their ability to generate original interconnected macroporous structures with the potential to influence cell behaviour, namely a network of spherical pores (impregnation of polymeric structure, PS), a network of interconnected diamond shaped pores (stereolithography, 3D) and a network of parallel ellipsoidal channel-like pores (freeze casting, FC). Porosity was higher on PS samples (~65%) and similar on 3D and FC samples (~50%). The latter two samples presented the lowest and the highest surface area,

respectively.

Proliferation occurred on every single material sample after a latency period (3–7 days) caused by a deleterious environment for cell adhesion and proliferation due to the dynamics of dissolution (material leaching)/precipitation (ion and protein deposition) events (data not shown) leading to the progressive development of a conditioning layer [49,50]. FC samples presented a longer lag phase, an expected behaviour considering its higher surface area thus a slower surface conditioning [49,50]. However, after stabilisation of the interface (material/biological fluids), the remaining living cells proliferated. It seems that confluence was met around the 28th day for the samples and at the 21st day for the control. 3D samples hosted the highest number of cells (similar to control). The grooves on 3D surface had a positive impact on cell adhesion and proliferation. This phenomenon is known as curvature driven growth [39]. They were followed by PS and FC. Besides the maximum proliferation values, the cell growth rate during the culture period was also an important issue in the cell/surface interaction. Control cultures presented a steady increase in the cell number however cell growth rate on the samples was higher between the 14th and 21st days (due to the initial lag phase). The latter was similar on PS and 3D samples (~3 fold increase), but it was much more significant on FC samples (~7 fold increase).

Quantitative PCR analysis for the expression of osteoblastic genes was done on the 14th day of culture, at an early proliferative stage. It shows that cell differentiation had occurred on every sample. As a whole, gene expression was higher on the β-TCP samples compared to control, indicating an increased differentiation, which is in line with the reported osteogenic inductive effect of β-TCP on HMSC [2,4,51]. BGLAP (osteocalcin) expression indicates that most of the cells on the scaffolds presented a mature phenotype, as it is a late osteoblastic differentiation marker [52]. However, expression levels of Runx-2, BMP-2 and ALP were greatly stimulated on FC compared to those on PS and 3D, suggesting that osteoblastic differentiation was enhanced on the freeze casted samples. Runx-2 is a key transcription factor that induces a program of gene expression required for osteogenic lineage commitment and differentiation of mesenchymal stem cells and is also required for osteoblastic functions beyond differentiation [52]. BMP-2 signalling pathway is essential for osteogenic differentiation and necessary for Runx-2-dependent induction of osteogenic gene expression. Thus, BMP-2 is suggested to have a dual effect; it is upstream of Runx-2 transcription but can team up with Runx-2 to regulate transcription of its target genes [52]. ALP expression is an early marker of osteogenic commitment and has a key role in the onset of matrix mineralization [52].

Alkaline phosphatase activity was measured over a period of 7 days beginning at the 21st day of culture, a phase of active proliferation, on confluent cultures. Two patterns were identified. First of all, the material itself, β-TCP, allowed higher enzymatic activity compared to the control. However, samples such as PS and 3D yielded stable values over the course of the test whereas the frozen sample showed an increase in enzymatic activity between the 21st and the 28th day. During the same time period, cell proliferation increased rapidly. It is clear that during this time period, from day 14–21, biological changes occurred. The maximum enzyme activity on the freeze casted samples (reached on the 28th day) was at least 2 fold the value yielded by the control on day 28. Alkaline phosphatase activity did not seem to be population-dependent as the largest cell population was present on 3D and on the control. However, freeze casted samples favoured alkaline phosphatase activity. As the latter is considered a differentiation marker for osteoblastic differentiation it was hypothesized that freeze casting samples improve HMSC differentiation compared to the other macroporous samples [53,54].

Enzymatic activity and SEM imaging confirm matrix mineralization which suggests a higher degree of cell differentiation and maturation.

These biological differences between samples can be attributed to the shaping methods chosen. Each of them yielded very specific macroporous architectures with features prone to influence proliferation and differentiation.

3D samples exhibited grooves on its surface thus stimulating cell growth and alignment. This regular micro texturing contributed to a large cell population to grow almost exclusively on the surface with poor migration inside the porous structure. Cell proliferation has been supported by curvature driven growth [39]. The rapid cell growth on the scaffold outer surface, leading to pore occlusions, has been suggested as a problem in tissue engineering as this behaviour restricts cell penetration [55]. In line with this, SEM images showed that cell migration into the 3D scaffold was mainly seen associated with pore corners, an expected behaviour, due to the local favoured curvature-driven cell/material interactions [55]. Images also suggested that, as a whole, the porous geometry, the small and the long pore diameters and the smooth pore surface topography, contrasting with the rough outer surface, did not seem appealing for cell migration and pore colonization. Inside the porous structure, cells behaved mostly as on a two-dimensional structure being unable to establish competent cell-to-cell communication and cell/material interactions leading to the formation of organized three-dimensional cellular-matrix constructs.

In terms of cellular performance, PS sample displayed a similar behaviour to that of the 3D samples. Cell growth was seen only on the outer surface, also leading to pore occlusion. The absence of surface aligned groves explains the lower proliferation values. Compared to 3D sample, the porous features of PS sample seemed worse, as cell migration was virtually absent. The comparatively sharper surface discontinuities produced by the pores might have played a role. Furthermore, the circular-shaped pore with a large diameter and the smooth pore topography introduced drastic changes in the substrate geometry and topography, respectively, which did not favour cellular migration [55]. Another adverse geometric feature appears to be the relatively long distance between the pore interconnection that, in the absence of anchoring topographic features, induced difficult surface topography-driven cell growth, preventing cellular infiltration.

FC exhibited channel-like ellipsoidal pores, with elongated and oriented pores randomly connected by orthogonal channels. The narrow pores and the acute angles induced confinement thus a favourable environment as interactions between cells and between cells and material increased. The pores' wall presented a lamellar morphology (seen as periodic protrusions) that induced cell elongation and continuous directional growth. This sample also exhibited texturized pore walls. These micrometric structures contributed to cell adhesion and reptation inside the pore network, as they provided anchoring sites for cell filopodia continuously probing the local environment aiding in cell tension-induced material invasion. Micro topography also increased surface area favouring ionic dissolution and re-precipitation events leading to the deposition of an apatite layer that, together with co-precipitated proteins, promotes cell growth and osteogenic differentiation [55]. As a result of these architectural features, massive cellular colonization of the entire porous scaffold is observed, contrasting with the almost exclusive outer surface cell growth that occurred on PS and 3D samples. Within the FC scaffold, the porous structure is completely filled with three-dimensional possibly mineralized cellular-matrix constructs, typical of the osteogenic differentiation of mesenchymal stem cells. This behaviour might explain the increased osteoblastic gene expression and ALP activity compared to PS and 3D. *In vivo*, survival, self-renewal and differentiation of stem cells are directed by local biochemical and mechanical factors within a local micro environmental niche [56]. The organization of the cellular constructs in the porous FC might suggest that this scaffold is endowed with niche-mimicking features.

Cell sensing and responsiveness to surface topography occur via mechanotransduction through the integrin receptors. These transmembrane receptors are critical communication channels that play a crucial role in the interaction of the cell with adjacent surfaces. Outside the cell, receptors bind to peptide ligands to modulate cell adhesion and the resulting intracellular tension triggers downstream biochemical signalling cascades, via the integrin-focal adhesion cytoskeleton pathway, affecting proliferation and differentiation [57,58]. Thus, changes in cell adhesion and cytoskeleton organization, in response to physical cues

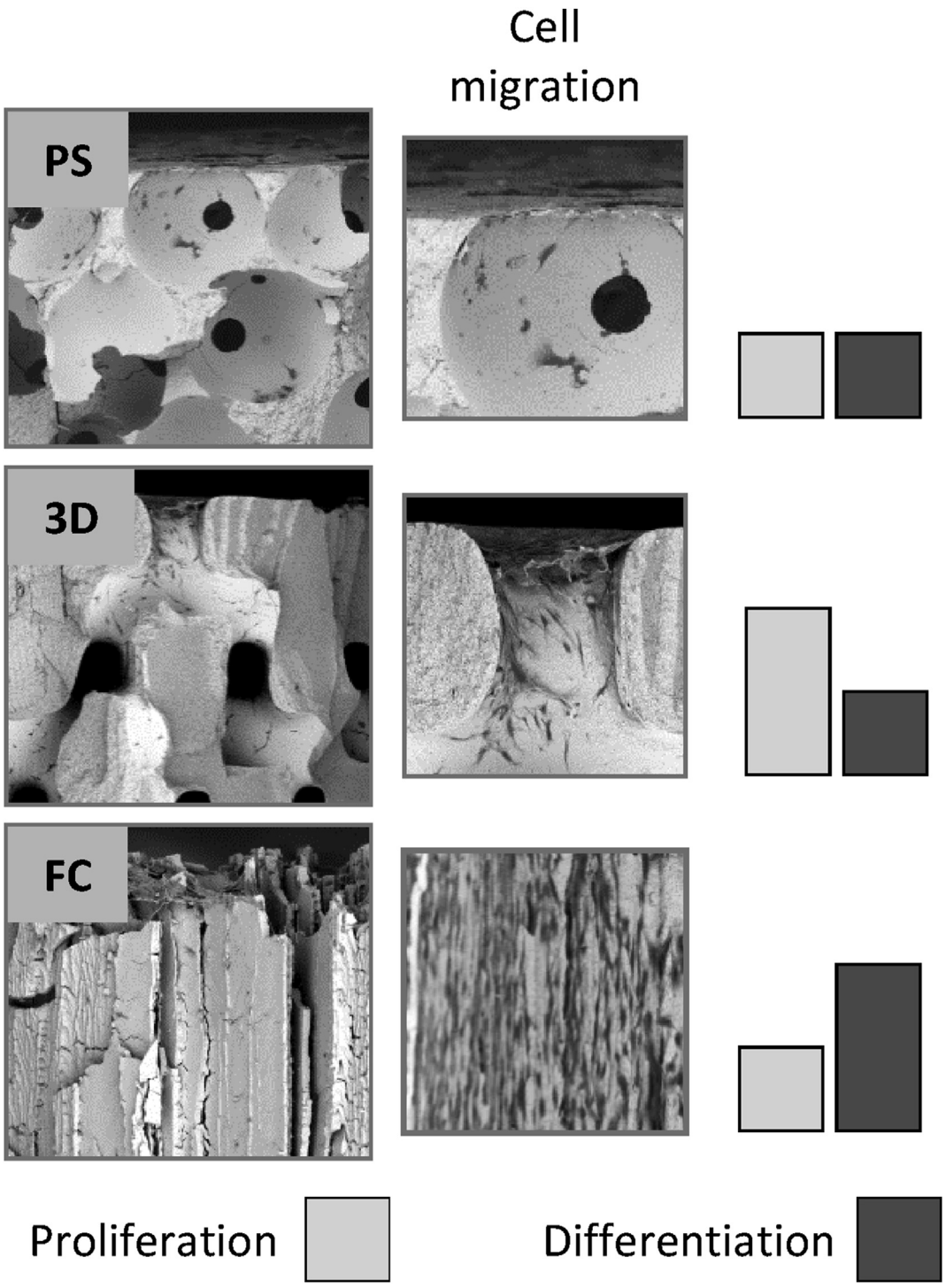

Fig. 10. SEM images of the β-TCP samples, and comparative cell behaviour.

such as topography, are essential to direct mechanotransductive processes. Related to this, it has been reported that microtopography could enhance integrin activation [59] and also improve cell behaviour via the activation of the BMP-2 signalling pathway [60]. Furthermore, studies suggested collaborative mechanisms between integrins and BMP-2 that could modulate both cell adhesion and osteogenic differentiation [61].

Taken together, results of this study suggest that the highly structured macroporous 3D and PS samples lacked the features that could potentially favour and/or increase cell differentiation and penetration inside the porous network. On the other hand, the high gradient of anisotropy of FC macro and microarchitecture provided continuous contact guidance cues inducing changes in cell mechanics, in particular spatial reorganization of the actin cytoskeleton, that sustain cell migration through cell-cell junctions with positive effects on cell growth and differentiation [55,62,63]. Fig. 10 sums up these observations.

5. Conclusion

During the course of this work, macroporous β-TCP bone implants were manufactured and tested *in vitro*. The different steps from the manufacturing of the β-TCP powder to its shaping were mastered.

Ceramic powder was made through aqueous precipitation and

complied with the ISO 13779 and 13,175 standards. The chosen shaping methods were: impregnation of a polymeric scaffold, stereolithography and freeze casting. The shaping processes were closely controlled and so were the pore sizes and interconnections. Each sample exhibited a different architecture with specific features that would subsequently influence HMSC development.

HMSC at the osteoprogenitor stage were used for *in vitro* testing. Cell proliferation took place over every single sample. 3D exhibited the largest population because of particular topographic features that induced curvature driven growth. However, cells would remain on the surface with very few individuals inside the porous structure. The same remarks can be made for PS. On the other hand, samples yielded by freeze casting favoured cell penetration and promoted osteoblastic differentiation genes expression as well as an increase in activity of alkaline phosphatase. Architectural features such as pore shape and size, surface and pore topographical features and specific surface have positively influenced cell behaviour. Through these results it seems clear that freeze casting is a shaping technique fit for the elaboration of structures that will contribute to cell invasion and differentiation. It might be worth using freeze casting as an inspiration for porous structures manufactured by techniques free of its constraints.

Declaration of competing interest

The authors declare that they have no known competing financial interests or personal relationships that could have appeared to influence the work reported in this paper.

Acknowledgement

This work was financially supported by the following entities: the Région Hauts-de-France, Valutec S.A, the JECS trust and the COST action. The authors would like to acknowledge and thank Pr. Francis Cambier and Dr. Dominique Hautcoeur of the Belgian Ceramic Research Centre for their help. The authors would also like to acknowledge and thank Mr. Vincent Hornez of Cryoceram for the manufacturing of the 3D samples.

References

[1] K. De Groot, Bioceramics consisting of calcium phosphates salts, Biomaterials 1 (1980) 47–50, 47.
[2] G. Hannink, J.J. Chris Arts, Bioresorbability, porosity and mechanical strength of bone substitutes: what is optimal for bone regeneration? Injury, Bone Substitutes: A Comprehensive Overview 42 (Supplement 2) (2011).
[3] M.R. Urist, Bone : formation by autoinduction, Science, New series 150 (No. 3698) (1965) 893–899.
[4] L. Cheng, T. Wang, J. Zhu, P. Cai, Osteoinduction of calcium phosphate ceramics in four kinds of animals for 1 Year: dog, rabbit, rat, and mouse, Transplant. Proc. 48 (4) (2016) 1309–1314.
[5] K.F. Leong, C.M. Cheah, C.K. Chua, Solid freeform fabrication of three-dimensional scaffolds for engineering replacement tissues and organs" Biomaterials, Focus on Biomaterials Science in Asia 24 (13) (2003) 2363–2378.
[6] E. Cukierman, R. Pankov, D.R. Stevens, K.M. Yamada, Taking cell-matrix adhesions to the third dimension, Science 294 (2001) 1708–1712.
[7] G. Kumar, C.K. Tison, K. Chatterjee, P.S. Pine, J.H. McDaniel, M.L. Salit, M.F. Young, C.G. Simon Jr., The determination of stem cell fate by 3D scaffold structures trough the control of cell shape, Biomaterials 32 (2011) 9188–9196.
[8] E.A. dos Santos, M. Farina, G.A. Soares, K. Anselme, Surface energy of hydroxyapatite and beta-tricalcium phosphate ceramics driving serum protein adsorption and osteoblast adhesion, J. Mater. Sci. Mater. Med. 19 (2008) 2307–2316.
[9] K. Lee, E.A. Silva, D.J. Mooney, Growth factor delivery-based tissue engineering: general approaches and a review of recent developments, J. R. Soc. Interface 8 (55) (2011) 153–170.
[10] W.L. Murphy, T.C. McDevitt, A.J. Engler, Materials as stem cell regulators, Nat. Mater. 13 (6) (2014) 547–557.
[11] J.C. Le Huec, T. Schaeverbeke, D. Clément, J. Faber, A. Le Rebeller, Influence of porosity on the mechanical resistance of hydroxyapatite ceramics under compressive stress, Biomaterials 16 (1995) 113–118.
[12] O. Gauthier, J.M. Bouler, E. Aguado, P. Pilet, G. Daculsi, Macroporous biphasic calcium phosphate ceramics: influence of macropore diameter and macroporosity percentage on bone ingrowth, Biomaterials 19 (1–3) (1998) 133–139.
[13] M.C. Kruyt, W.J.A. Dhert, C. Oner, C.A. van Blitterswijk, A.J. Verbout, J.D. de Bruin, Optimization of bone-tissue engineering in goats, J. Biomed. Mater. Res. B Appl. Biomater. 69B (2004) 113–120.
[14] J.H. Park, J.Y. Bae, J. Shim, I. Jeon, Evaluation of suitable porosity for sintered porous ? tricalcium phosphate as a bone substitute, Mater. Char. 71 (2012) 103–111.
[15] F. Pecqueux, F. Tancret, N. Payraudeau, J.M. Bouler, Influence of microporosity and macroporosity on the mechanical properties of biphasic calcium phosphate bioceramics: modelling and experiment, JECS 30 (4) (2010) 819–829.
[16] F.J. O'Brien, B.A. Harley, I.V. Yannas, L.J. Gibson, The effect of pore size on cell adhesion in collagen-GAG scaffolds, Biomaterials 26 (4) (2005) 433–441.
[17] S.F. Hulbert, F.A. Young, R.S. Mathews, J.J. Klawitter, C.D. Talbert, F.H. Stelling, Potential of ceramic materials as permanently implantable skeletal protheses, J. Biomed. Mater. Res. 4 (3) (1970) 433–456.
[18] B. Flautre, M. Descamps, C. Delcourt, M.C. Blary, P. Hardouin, Porous HA ceramic for bone replacement: role of the pores and interconnections - Experimental study in rabbit, J. Mater. Sci. Mater. Med. 12 (2001) 679–682.
[19] A.C. Jones, C.A. Arns, D.W. Hutmatcher, B.K. Milthorpe, A.P. Sheppard, M.A. Knackstedt, The correlation of pore morphology, interconnectivity and physical properties of 3D ceramic scaffolds with bone ingrowth, Biomaterials 30 (2009) 1440–1451.
[20] B.S. Chang, K.S. Hong, H.J. Youn, H.S. Ryu, S.S. Chung, K.W. Park, Osteoconduction at porous hydroxyapatite with various pore configurations, Biomaterials 21 (12) (2000) 1291–1298.
[21] L. Galois, D. Mainard, Bone ingrowth into two porous ceramics with different pore sizes: an experimental study, Acta Orthop. Belg. 70 (2004) 598–603.
[22] V. Karageorgiou, D. Kaplan, Porosity of 3D biomaterial scaffolds and osteogenesis, Biomaterials 26 (27) (2005) 5474–5491.
[23] E. Tsuruga, H. Takita, H. Itoh, Y. Wakisaka, Y. Kuboki, Pore size of porous HA as the cell-substratum controls BMP-induced osteogenesis, J. Biochem. 121 (1997) 317–324.
[24] Y. Kuboki, Q. Jin, H. Takita, Geometry of carriers controlling phenotypic expression in BMP induced osteogenesis and chondrogenesis, J Bone Surg Am 83 (1 suppl 2) (2001) 105–115.
[25] R.A.D. Carano, E.H. Filvaroff, Angiogenesis and bone repair, DDT 8 (2003) 980–989, 21.
[26] S.M. Mantila Roosa, J.M. Kemppainen, E.N. Moffitt, P.H. Krebsbach, S.J. Hollister, The pore size of polycaprolactone scaffolds has limited influence on bone regeneration in an in vivo model, J. Biomed. Mater. Res. (2009) 359–368.
[27] J.C. Hornez, F. Chai, F. Monchau, N. Blanchemain, M. Descamps, H.F. Hildebrand, Biological and physico-chemical assessment of hydroxyapatite (HA) with different porosity, Biomol. Eng. 24 (5) (2007) 505–509.
[28] J.R. Woodard, A.J. Hilldore, S.K. Lan, C.J. Park, W.A. Morgan, J.A.C. Eurell, A.J. Wagoner Jonhson, The mechanical properties and osteoconductivity of hydroxyapatite bone scaffolds with multi-scale porosity, Biomaterials 28 (1) (2007) 45–54.
[29] C. Wang, Y. Dua, B. Markovic, J. Barbara, C. Rolfe Howlett, X. Zhang, H. Zreiqat, Proliferation and bone-related gene expression of osteoblasts grown on HA ceramics sintered at different temperature, Biomaterials 25 (15) (2004) 2949–2956.
[30] P. Frayssinet, N. Rouquet, J. Fages, M. Durand, P.O. Vidalain, G. Bonel, The influence of sintering temperature on the prolifération of fibroblastic cells in contact with HA bioceramics, J. Biomed. Mater. Res. 35 (1997) 337–347.
[31] F.M. Klenke, Y. Liu, H. Yuan, E.B. Hunziker, A.K. Siebenrock, W. Hofstetter, Impact of pore size on the vascularization and osseointegration of ceramic bone substitutes in vivo, J. Biomed. Mater. Res. 85 (3) (2008) 777–786.
[32] A. Bignon, J. Chouteau, J. Chevalier, G. Fantozzi, J.P. Carret, P. Chavassieux, G. Boivin, M. Melin, D. Hartmann, Effect of micro- macroporosity of bone substitutes on their mechanical properties and cellular response, J. Mater. Sci. Mater. Med. 14 (2003) 1089–1097.
[33] A. Curtis, C. Wilkinson, Topographical control of cells, Biomaterials 18 (1997) 1573–1583.
[34] A. Carvalho, A. Pelaez-Vargas, D.J. Hansford, M.H. Fernandes, F.J. Monteiro, Effects of line and pillar array microengineered SiO2 thin films on the osteogenic differentiation of human bone marrow derived MSC, Langmuir 32 (4) (2016) 1091–1100.
[35] A.B. Faia-Torres, M. Charnley, T. Goren, S. Guimond-Lischer, M. Rottmar, K. Maniura-Weber, N.D. Spencer, R.L. Reis, M. Textor, N.M. Neves, Osteogenic differentiation of HMSC in the absence of osteogenic supplements, Acta Biomater. 28 (C) (2015) 64–75.
[36] B. Li, X. Liao, L. Zheng, X. Zhu, Z. Wang, H. Fan, X. Zhang, Effect of nanostructure on osteoinduction of porous biphasic calcium phosphate ceramics, Acta Biomater. 8 (2012) 3789–3804.
[37] T.J. Webster, C. Ergun, R.H. Doremus, R.W. Siegel, R. Bizios, Specific proteins mediate enhanced osteoblast adhesion on nanophase ceramics, J. Biomed. Mater. Res. 51 (2000) 475–483.
[38] J. Knychala, N. Bouropoulos, C.J. Catt, O.L. Katsamenis, C.P. Please, B.G. Sengers, Pore geometry regulates early stage human bone marrow cell tissu formation and organisation, Ann. Biomed. Eng. 41 (2013) 917–930.
[39] C.M. Bidan, K.P. Kommareddy, M. Rumpler, P. Kollmannsberger, Y.J.M. Bréchet, P. Fratzl, J.W.C. Dunlop, How linear tension converts to curvature: geometric control of bone tissue growth, PloS One 7 (2012), e36336.
[40] C.M. Bidan, K.P. Kommareddy, M. Rumpler, P. Kollmannsberger, P. Fratzl, J.W.C. Dunlop, Geometry as a factor for tissue growth: towards shape optimization of tissue engineering scaffolds, Adv Healthc Mater 2 (2013) 186–194.
[41] M. Rumpler, A. Woesz, J.W.C. Dunlop, J.T. van Dongen, P. Fratzl, The effect of geometry on three dimensional tissue growth, J R Interface 5 (2008) 1173–1180.

[42] E.R. Urquia Edreira, A. Hayrapetyan, J.G.C. Wolke, H.J.E. Croes, A. Klymov, J.A. Jansen, J.J.J.P. vanden Beucken, Effect of calcium phosphate ceramic substrate geometry on MSC organization and osteogenic differentiation, Biofabrication 8 (2016), 025006.
[43] L. Juignet, B. Charbonnier, V. Dumas, W. Bouleftour, M. Thomas, C. Laurent, L. Vico, N. Douard, D. Marchat, L. Laval, Macrotopographic closure promotes tissue growth and osteogenesis in vitro, Acta Biomater. 53 (2017) 536–548.
[44] A.R. Studart, U.T. Gonzenbach, E. Tervoort, L.J. Gauckler, Processing routes to macroporous ceramics: a review, J. Am. Ceram. Soc. 89 (2006) 1771–1789, 6.
[45] T. Ohiji, M. Fukushima, Macroporous ceramics: processing and properties, Int. Mater. Rev. 57 (2) (2012) 115–131.
[46] M. Descamps, T. Duhoo, F. Monchau, J. Lu, P. Hardouin, J.C. Hornez, A. Leriche, Manufacture of macroporous β-tricalcium phosphate bioceramics, J. Eur. Ceram. Soc. 28 (1) (2008) 149–157.
[47] S. Deville, Freeze casting of porous ceramics: a review of current achievement and issues, Adv. Eng. Mater. 10 (3) (2008) 155–169.
[48] S. Raynaud, E. Champion, D. Bernache-Assolant, J. Laval, Determination of calcium/phosphorus atomic ratio of calcium phosphate apatites using X-ray diffractometry, J. Am. Ceram. Soc. 84 (2001) 355–366.
[49] A. John, H.K. Varma, T.V. Kumari, Surface reactivity of calcium phosphate based ceramics in a cell culture system, J. Biomater. Appl. 18 (2003) 63–78.
[50] M. Kamitakahara, C. Ohtsuki, T. Miyazaki, Review paper: behavior of ceramic biomaterials derived from tricalcium phosphate in physiological condition, J. Biomater. Appl. 23 (2008) 197–212.
[51] R.Z. LeGeros, Calcium phosphate-based osteoinductive materials, Chem. Rev. 108 (2008) 4742–4753.
[52] E.D. Jensen, R. Gopalakrishnan, J.J. Westendorf, Regulation of gene expression in osteoblasts, BioFactors NA-NA, 2010.
[53] J.E. Aubin, Regulation of osteoblast formation and function, Rev. Endocr. Metab. Disord. 2 (1) (2001) 81–94.
[54] P. Marie, Différenciation, fonction et controle de l'ostéoblaste, Medecine/Sciences, 2001, pp. 1252–1259.
[55] M.I. Gariboldi, S.M. Best, Effect of ceramic scaffold architectural parameters on biological response, Frontiers in Bioengineering and Biotechnology 3 (2015).
[56] D.E. Discher, D.J. Mooney, P.W. Zandstra, Growth factors, matrices, and forces combine and control stem cells, Science 324 (2009) 1673–1677.
[57] C.H. Seo, K. Furukawa, K. Montagne, H. Jeong, T. Ushida, The effect of substrate microtopography on focal adhesion maturation and actin organization via the RhoA/ROCK pathway, Biomaterials 32 (2011) 9568–9575.
[58] C. Zhao, X. Wang, L. Gao, L. Jing, Q. Zhou, J. Chang, The role of the micro-pattern and nano-topography of hydroxyapatite bioceramics on stimulating osteogenic differentiation of mesenchymal stem cells, Acta Biomater. 73 (2018) 509–521.
[59] R. Olivares-Navarrete, S.L. Hyzy, M.E. Berg, J.M. Schneider, K. Hotchkiss, Z. Schwartz, B.D. Boyan, Osteoblast lineage cells can discriminate microscale topographic features on Ti–Al–V surfaces, Ann. Biomed. Eng. 42 (2014) 2551–2561.
[60] Z. Chen, C. Wu, W. Gu, T. Klein, R. Crawford, Y. Xiao, Osteogenic differentiation of bone marrow MSCs by β-tricalcium phosphate stimulating macrophages via BMP2 signalling pathway, Biomaterials 35 (2014) 1507–1518.
[61] Z. Mai, Z. Peng, S. Wu, J. Zhang, L. Chen, H. Liang, D. Bai, G. Yan, H. Ai, Single bout short duration fluid shear stress induces osteogenic differentiation of MC3T3-E1 cells via integrin β1 and BMP2 signaling cross-talk, PloS One 8 (2013), e61600.
[62] D.H. Kim, C.H. Seo, K. Han, K.W. Kwon, A. Levchenko, K.Y. Suh, Guided cell migration on microtextured substrates with variable local density and Anisotropy, Adv. Funct. Mater. 19 (2009) 1579–1586.
[63] M.M. Silva, L.A. Cyster, J.J. Barry, X.B. Yang, R.O. Oreffo, D.M. Grant, C.A. Scotchford, S.M. Howdle, The effect of anisotropic architecture on cell and tissue infiltration into tissue engineering scaffolds, Biomaterials 27 (2006) 5909–5917.